ISSN 0001-4338, Izvestiya, Atmospheric and Oceanic Physics, 2013, Vol. 49, No. 5, pp. 485–493. © Pleiades Publishing, Ltd., 2013.
Original Russian Text © D.A. Smirnov, I.I. Mokhov, 2013, published in Izvestiya AN. Fizika Atmosfery i Okeana, 2013, Vol. 49, No. 5, pp. 530–539.

Estimation of Interaction between Climatic Processes: Effect of Sparse Sample of Analyzed Data Series

D. A. Smirnov[a] and I. I. Mokhov[b]

[a] *V.A. Kotel'nikov Institute of Radio Engineering and Electronics, Saratov Department, ul. Zelenaya 38, Saratov, 410019 Russia*
e-mail: smirnovda@yandex.ru

[b] *A.M. Obukhov Institute of Atmospheric Physics, Russian Academy of Sciences, per. Pyzhevskii 3, Moscow, 119017 Russia*
e-mail: mokhov@ifaran.ru

Received October 29, 2012; in final form, February 28, 2013

Abstract—It is shown that the approach based on the Granger causality may lead to erroneous conclusions about bidirectional coupling (BC) in the case of unidirectional coupling (UC) and quite a sparse sample of the data series analyzed. This effect was revealed in an analysis of coupling between variations in the solar irradiance and global surface temperature. We present a statistical test to confirm or reject speculations about the character (unidirectional or bidirectional) of coupling. The corresponding analysis of coupling between phenomena of El Niño and the Indian Monsoon confirmed the earlier conclusions about their mutual influence.

Keywords: time series, estimates of couplings, unidirectional coupling, bidirectional coupling, Granger causality, temperature, solar activity, El Niño, Southern Oscillation, Indian Monsoon

DOI: 10.1134/S0001433813050113

1. INTRODUCTION

Researchers have become increasingly concerned not only about couplings between different global and regional climate processes, but also about the direction of influence, which may not be unidirectional and may vary in time and, in particular, due to external natural and anthropogenic effects [1–28]. A useful approach to studying the cause-and-effect relationships in the earth's climate system is one based on the notion of Granger causality [29], making it possible to estimate the degree of the mutual effect of climate processes taking into account external impacts (see, e.g., [13, 14, 18, 19, 21, 23, 25, 26, 28]). Coupling between two processes may be either unidirectional (UC), when one of two processes influences the other, or bidirectional (BC), with mutual effect, such as was identified in an analysis of Granger causality for phenomena of El Niño and the Indian Monsoon [25, 26].

System Y influences system X according to Granger if the future behavior of X is better predicted when data on Y are incorporated than when data on X alone are used. The nonzero improvement of prediction (IP) is associated with the presence of influence of Y on X, and nonzero IPs in both directions are usually interpreted as BC signature. It is noteworthy that the prediction is performed one time step Δt, i.e., sampling interval, ahead. However, the IP may depend on Δt in a complex way, and works [30, 31] noted that, for quite a sparse sample, and even in the case of unidirectionally coupled systems, nonzero IPs in both directions, i.e., "false couplings," may be observed. This key finding should be taken into account, in particular, in an analysis of climatic data.

In this paper we analyzed the effect of the sparse sample on the determination of the interrelation between processes according to time series of data on the basis of the Granger causality. The presence of this effect, leading to unreliable conclusions on BC, was identified in a study of variations in global surface temperature (GST) and solar radiative flux. The possibility for misidentification is demonstrated with reference stochastic systems with UC as an example. We present a statistical test for distinguishing between UC and BC based on accounting for the effect of the sparse sample. This test is used to verify the conclusion about BC between the El Niño Southern Oscillation (ENSO) and the Indian Monsoon [25, 26].

2. GRANGER CAUSALITY

Let $(X(t), Y(t))$ be a two-dimensional random process, the realizations of which are recorded at discrete times with the sampling interval Δt: $x_n = X(n\Delta t)$, $y_n = Y(n\Delta t)$, where n is an integer. We can introduce notations $x_n^- = \{x_{n-k}\}_{k=1}^{\infty}$ and $y_n^- = \{y_{n-k}\}_{k=1}^{\infty}$ for the sets of x and y values until the time n. Among all other possible methods for an individual (without accounting for Y) prediction of x_n, the least standard error is

achieved at $x_n^{ind} = M\left[x_n \middle| x_n^-\right]$, where $M\left[x_n \middle| x_n^-\right]$ means the conditional mathematical expectation of x_n conditioned upon x_n^-. The variance of this error will be denoted through $\sigma_{x,ind}^2 = M[(x_n - x_n^{ind})^2]$. The best joint (with accounting for Y) prediction is given by the formula $x_n^{joi} = M\left[x_n \middle| x_n^-, y_n^-\right]$; it has the error with the variance $\sigma_{x,joi}^2 = M[(x_n - x_n^{joi})^2]$. The normalized IP value $G_{y\to x} = (\sigma_{x,ind}^2 - \sigma_{x,joi}^2)/\sigma_{x,ind}^2$ characterizes the Granger causality (influence) in the direction $Y \to X$. The influence $X \to Y$ is defined analogously.

This approach was first implemented in [29] for stationary Gaussian processes (x_n, y_n). It was considered that this process is uniquely described by two-dimensional linear autoregression (AR) equation of the form

$$\begin{aligned} x_n &= \sum_{k=1}^{\infty} a_{x,k} x_{n-k} + \sum_{k=1}^{\infty} b_{x,k} y_{n-k} + \xi_n, \\ y_n &= \sum_{k=1}^{\infty} a_{y,k} y_{n-k} + \sum_{k=1}^{\infty} b_{y,k} x_{n-k} + \psi_n, \end{aligned} \tag{1}$$

where (ξ_n, ψ_n) is a two-dimensional Gaussian white noise with zero mean, respective variances of components σ_ξ^2 and σ_ψ^2, and covariance $M[\xi_n \psi_n] = \gamma$. The condition that the noise is "white" is equivalent to the minimum of prediction error [32], with $\sigma_\xi^2 = \sigma_{x,joi}^2$ and $\sigma_\psi^2 = \sigma_{y,joi}^2$. Further, the process x_n obeys the one-dimensional AR equation, i.e., the first equation in (1) with zero $b_{x,k}$ and white noise ξ'_n, the variance of which $\sigma_{\xi'}^2 = \sigma_{x,ind}^2$. Now the variances of the noises σ_ξ^2, $\sigma_{\xi'}^2$ are used to determine IP $G_{y\to x}$. Analogously, we determine $G_{x\to y}$.

In order to estimate the theoretical quantities $G_{y\to x}$ and $G_{x\to y}$ for a finite time series $\{x_n, y_n\}_{n=1}^N$, all sums in Eqs. (1) are restricted to the term $k = p$ (instead of $k = \infty$), and the coefficients and variances of noises in AR models of order p are estimated with the help of the standard least squares method. In the numerical examples analyzed below, the length N of the series is large; therefore, the p value is chosen to be just great enough that the estimation results practically no longer change with the further p increase (namely, $p = 10$ was found to be sufficient in all examples considered here). The Schwarz criterion [33] is used in an analysis of the climatic time series when polynomial order is selected. The statistical significance of nonzero $G_{y\to x}$ and $G_{x\to y}$ estimates is verified with the help of the Fisher F-test [34].

It should be noted that Eqs. (1) for different Δt are different valid representations of the initial system (X, Y). Then how do $G_{y\to x}$ and $G_{x\to y}$ change with variations in Δt? If there is no real influence $Y \to X$, it would be reasonable to expect that $G_{y\to x} = 0$ for any Δt, or at least that $G_{y\to x} \ll 1$ and $G_{y\to x} < G_{x\to y}$. However, these expectations do not always come true [35] and, moreover, the relative measure of the "false causality" $r = G_{y\to x}/G_{x\to y}$ may substantially exceed unity.

3. EFFECT OF SPARSE SAMPLE

To evaluate the influence of the sampling interval on the estimation of couplings, we analyzed the stochastic linear dissipative oscillators with discrete time:

$$\begin{aligned} X(t) &= A_{X,1} X(t-1) + A_{X,2} X(t-2) + B_X Y(t-1) + \Xi(t), \\ Y(t) &= A_{Y,1} Y(t-1) + A_{Y,2} Y(t-2) + B_Y X(t-1) + \Psi(t), \end{aligned} \tag{2}$$

where Ξ, Ψ are independent Gaussian white noises with zero means and variances σ_Ξ^2 and σ_Ψ^2, B_X and B_Y are the coupling coefficients. The intrinsic oscillation period of X (position of the peak in the power spectrum) and its relaxation time (which determines the width of the peak) are given by the formulas $A_{X,1} = 2\cos(2\pi/T_X)\exp(-1/\tau_X)$ and $A_{X,2} = -\exp(-2/\tau_X)$ [36]. Formulas for Y look similar. We used the oscillation periods $T_X = T_Y = 4.4$, relaxation times $\tau_X = \tau_Y = 4$, variances of the noises $\sigma_\Xi^2 = \sigma_\Psi^2 = 1$, and the coupling coefficients $B_X = 0$ and $B_Y = 0.3$ (UC $X \to Y$) as the initial values for analysis. The IP values were estimated on the basis of time series of quite a large length $N = 10^5$, so the statistical fluctuations were negligibly small. Figure 1 (circles) demonstrates that UC is adequately characterized by IP at $\Delta t = 1$: $G_{y\to x} = 0$ and $G_{x\to y} > 0$. However, as Δt grows, the values of $G_{y\to x}$, also become positive and this "false coupling" is just a manifestation of the effect of a sparse sample. The value of $G_{y\to x}$ is maximal at $\Delta t = 3$, where $r = 0.1$ means that IP in the direction $Y \to X$, not corresponding to the real influence, is quite large at 10% of that in the direction of real influence $X \to Y$. As $\Delta t \to \infty$, the dependence between x and y values at very strongly separated consecutive times disappears, so that $G_{y\to x}$, $G_{x\to y}$ are close to zero (see Figs. 1a and 1b at $\Delta t = 15$), implying that the process (x_n, y_n) becomes white noise.

For interpreting nonzero $G_{y\to x}$ at $\Delta t > 1$, it should be noted that X is a second-order Markov process and the vector $(X(t), X(t-1))$ contains complete information on the distribution of future values $X(t+l)$ for any $l > 0$. In this case, $(X(t), X(t-1))$ totally determines the state of the process X at time t, with no IP of the process X if Y is taken into consideration. For $\Delta t > 1$ the prediction of $X(t+l)$ on the basis of $\{X(t),$

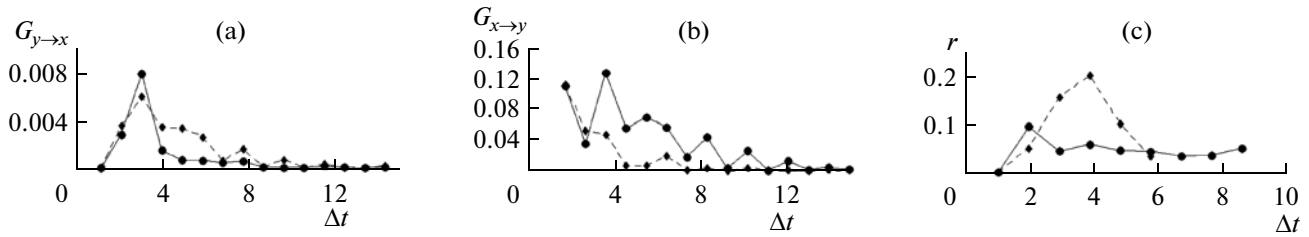

Fig. 1. Characteristics of Granger causality for unidirectionally coupled oscillators (2) at $T_X = T_Y = 4.4$ with downsampling (solid lines + circles) and with downsampling plus averaging (dashed lines + diamonds).

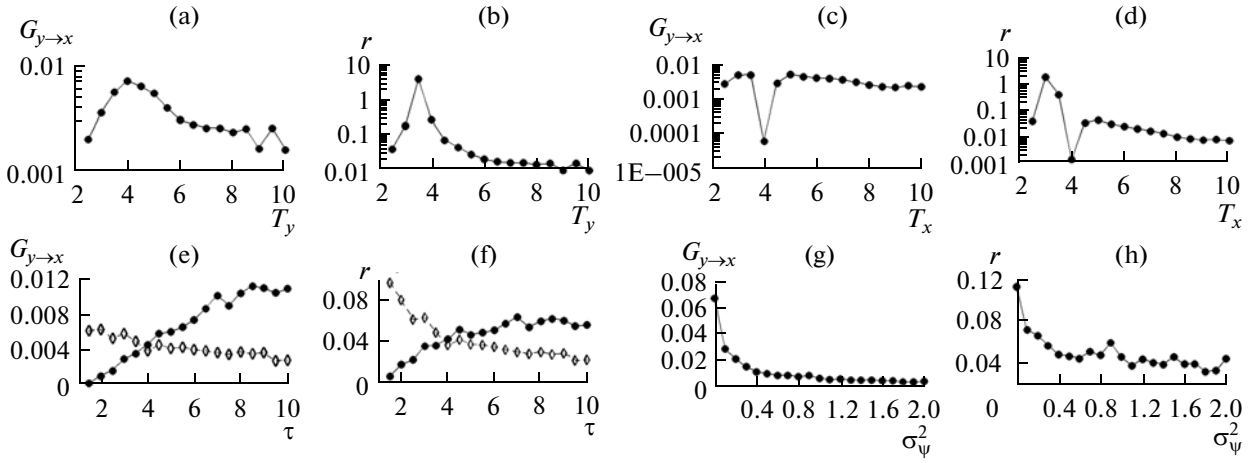

Fig. 2. Characteristics of Granger causality for unidirectionally coupled oscillators (2) as functions of different system parameters with the other kept fixed and taken from the base set $T_X = T_Y = 5$, $\tau_X = \tau_Y = 4$, $\sigma^2_\Xi = \sigma^2_\Psi = 1$, $B_X = 0$, $B_Y = 0.3$.. (e, f) $\tau = \tau_X$ (closed circles) and $\tau = \tau_Y$ (diamonds).

$X(t - \Delta t)$, $X(t - 2\Delta t)$, ...} is not the best, since the $X(t - 1)$ value cannot be retrieved exactly using downsampled data for X. At the same time, additional prognostic information can be obtained according to data on Y owing to the correlation existing between $X(t - 1)$ and observed Y values, thereby leading to positive IP of $G_{y\to x}$, not corresponding to the real influence. Thus, false couplings stem from incompleteness of information on the state of the master system in the data observed.

Positive values of $G_{y\to x}$ and r are found in wide ranges of parameter values, as is shown in Fig. 2, where $\Delta t = 2$ and where one of the parameters varies in each plot, while all the other parameters have fixed values taken out of the base set $T_X = T_Y = 5$, $\tau_X = \tau_Y = 4$, $\sigma^2_\Xi = \sigma^2_\Psi = 1$, $B_X = 0$, $B_Y = 0.3$. For small noises in the slave system σ^2_Ψ, states of the master system are better retrieved according to data on Y; as a consequence, we obtain large values for both $G_{y\to x} > 0.06$, and $r > 0.1$ (Figs. 2g, 2h). The ratio r exceeds unity for $T_X = 3$ (Fig. 2d) or $T_Y = 3.5$ (Fig. 2b). It should be noted that r is large for nonidentical oscillators (for $T_X \neq T_Y$, in the cases indicated above); for identical oscillators (i.e., for $T_X = T_Y$, $\tau_X = \tau_Y$, $\sigma^2_\Xi = \sigma^2_\Psi$) it remains within $r < 1$. Figures 2e and 2f indicate that r depends in different ways on two relaxation times: it grows with increasing τ_X and decreases with increasing τ_Y, the latter being because the information on the state of X is worse retrieved according to data on Y. Therefore, $G_{y\to x}$ and r have even larger values when the relaxation time is relatively large for the master system and small for the slave system. For instance, when $\tau_X = 10$, $\tau_Y = 1$, $\sigma^2_\Psi = 0.01$ and, with all the other parameters being those out of the base set, we have $G_{y\to x} = 0.14$ which exceeds all values in Fig. 2.

These results indicate that the effect of false couplings that arise due to a sparse sample is typical (shows up not only for some selected parameters) and may be very strong ($r > 1$). Both these conclusions are nontrivial and should be taken into consideration when real couplings are detected and analyzed. On the whole, it should be expected that, for systems with continuous time, the effect of a sparse sample may be

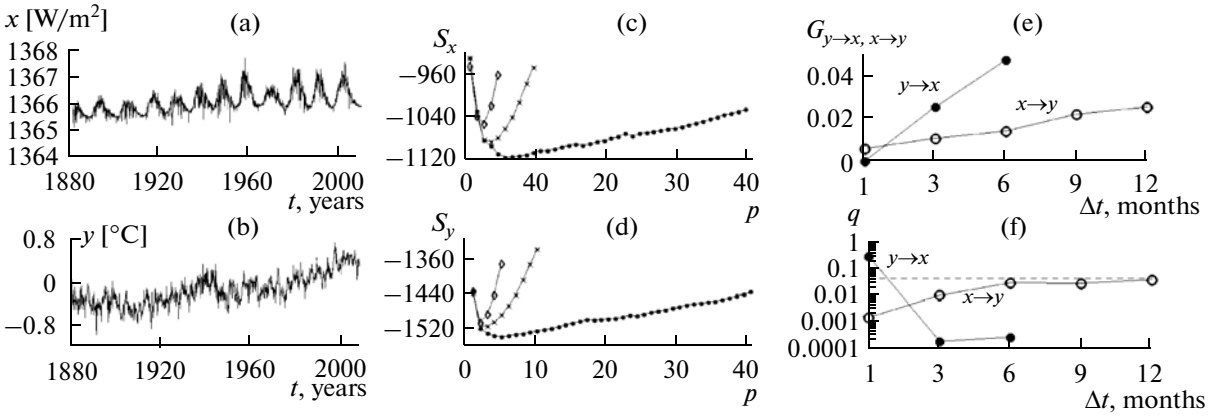

Fig. 3. Effect of sparse sample in analysis of coupling between (a) variations in the solar irradiance (solar constant) and (b) anomalies in the global near-surface temperature: (c, d) the corresponding dependences of the Schwarz criterion on the order of individual AR model with the polynomial on the order of one (circles), two (crosses), and three (diamonds); (e, f) the characteristics of Granger causality and the significance level of the conclusion about their positivity as functions of the sampling interval. The optimal values of AR orders: $p_x = 6$, 10, and 5 at $\Delta t = 1$, 3, and 6 and $p_y = 5$, 2, 4, 4, and 4 at $\Delta t = 1$, 3, 6, 9, and 12. At $\Delta t = 9$ and 12, the optimal values $p_x = 12$ and 9, even with $p_{xy} = 1$, give the number of coefficients greater than $\sqrt{N}$, so that IP estimates are untrustworthy (not shown). The dashed line indicates the level $q = 0.05$.

manifested for any sampling interval, because this just looks like downsampling. This is confirmed in numerical experiments dealing with analogous stochastic oscillators with continuous time. However, $G_{y\to x}$ diminishes with a decreasing sampling interval and is not accepted as significant anymore when estimated over a finite time series. In this regard, false couplings are practically manifested only for a sampling interval that is not too small, which depends on the length of the time series and theoretical value of $G_{y\to x}$.

The general conditions for the maximal manifestation of the effect of false couplings and its dependence on system parameters require special consideration. This effect is not necessarily associated with the relationship between the sampling frequency of the analyzed downsampled data and the Nyquist frequency for more detailed data. Its manifestation should depend on the relationship between sampling interval and key parameters of the studied system, including characteristic oscillation periods of oscillators. In accordance with the results obtained in this work and, in particular, for oscillators with nearly identical periods, the effect is maximal for the sampling interval in the range from 1/3 to 2/3 of the characteristic oscillation period. For the case, presented in Fig. 1a, with $T_X = 4.4$, this relationship, with the maximum for $\Delta t = 3$, is close to 2/3.

It should be noted that climatic studies consider not only downsampled data, but also data downsampled and averaged over the sampling interval (time step). For the initial system with discrete time, this reduces to the following manipulations:

$$x_n = \frac{1}{\Delta t}\sum_{i=1}^{\Delta t} X((n-1)\Delta t + i),$$
$$y_n = \frac{1}{\Delta t}\sum_{i=1}^{\Delta t} Y((n-1)\Delta t + i). \qquad (3)$$

The analogous effect of scarce sample takes place here. The values of "false couplings" for $G_{y\to x}$ turn out to be close to those in the case of ordinary downsampling, and may even exceed these latter (see results shown with diamonds in Fig. 1).

4. COUPLING OF VARIATIONS IN SOLAR RADIATION AND GNT

The effect of sparse sample for climate processes can be estimated by analyzing coupling between variations in the solar irradiance $x(t)$ and global surface temperature $y(t)$, the unidirectional character of which is known a priori. The influence $x \to y$ was obvious [18, 37, 38], while the influence $y \to x$ was unrealistic. The monthly ($\Delta t = 1$ month) data for $x(t)$ and $y(t)$, presented in Figs. 3a and 3b (see, e.g., http://climexp.knmi.nl), span the period of 1882–2008, i.e., $N = 1524$ months. The slow growth in both values may be due to the stochastic trend of stationary processes [3], suggesting that AR models are inapplicable of estimating Granger causality. Below we consider IP estimates based on the initial data, as well as those based on downsampled and averaged data according to (3) for the intervals $\Delta t = 3$, 6, 9, and

12 months with lengths of the corresponding time series of $N = 508$, 254, 169, and 127.

The Granger causality was estimated from time series of variations in the solar irradiance and global surface temperature using individual AR models with different orders of autoregression p and with polynomials of different orders K in the right-hand side. An optimal model of process x was selected according to Schwarz criterion [33] from the minimization condition $S_x = \frac{N}{2}\ln\sigma^2_{x,ind} + \frac{k}{2}\ln N$, where k is the number of coefficients to be estimated. Analogously, the individual orders and degrees were also selected for the process y. Linear models of x and y were always optimal for the data analyzed here; this can be seen from Figs. 3c and 3d for $\Delta t = 1$, where the optimal order of AR was $p_x = 6$, for x and $p_y = 5$ for y. To estimate $G_{y\to x}$ according to this same criterion, we selected the optimal number p_{xy} of accounted-for y values in the prediction of x. It was found to be unity in all cases, except at $\Delta t = 1$, where it was zero. Analogously, in the $G_{x\to y}$ calculation, the optimal number p_{yx} of included x values in the prediction of y was unity in all cases. It is noteworthy that the number of estimated coefficients in AR models should always be less than $\sqrt{N}$ for a sufficient statistic [25]; otherwise, the estimate of significance level according to the F-test is untrustworthy.

Thus, at $\Delta t = 1$ the $G_{y\to x}$ value statistically insignificantly differs from zero (an estimate of the significance level of q according to an F-test is much larger than 0.05; see Fig. 3f) for any nonzero p_{xy} (such as for $p_{xy} = 1$ in Fig. 3e); i.e., no false coupling $y \to x$ is identified. As to the opposite influence, the $G_{x\to y} = 0.006$ value is significantly positive at the level $q < 0.002$; i.e., the influence $x \to y$ is correctly identified according to monthly data. For $\Delta t > 1$, statistically significant IPs are recorded in both directions (Figs. 3e, 3f), once again exemplifying the effect of scarce sample. Thus, misidentifications of BC in an analysis of the climatic time series are quite possible and necessitate special verification.

5. TEST FOR BIDIRECTIONAL COUPLING

The results indicate that an analysis of time series $\{x_n, y_n\}_{n=1}^N$ provides no reliable answer about the presence of BC, even if both $G_{y\to x}$ and $G_{x\to y}$ estimates statistically significantly differ from zero. This conclusion can only be reached through a special test, rejecting or accepting the "zero hypothesis" about UC. In this case, the probability of erroneous rejection should not exceed some small value (significance level). We suggest, in particular, the following approach to testing [35]. Consider a certain class M of models for the process (X, Y) with UC and some "internal" time step, which is less than the sampling interval Δt. Within M, we search for a model capable of adequately reproducing the statistical characteristics of observed data (x_n, y_n). If this model exists, the UC hypothesis cannot be rejected (the test for BC fails). It should be underlined that the test is performed only on the basis of available data with sampling interval Δt, because data with a shorter sampling interval (as was the case in section 4) are usually unavailable. A shorter time step is used only in a model whose downsampled characteristics are comparable with their counterparts inferred from observation data.

This approach will be implemented by the example of stationary Gaussian processes with discrete time; for this we will consider the class M models of the form

$$\begin{aligned} X(t) &= \sum_{k=1}^{P} A'_{X,k} X(t - k\tau) + \sum_{k=1}^{S} B'_{X,k} Y(t - k\tau) + \Xi'(t), \\ Y(t) &= \sum_{k=1}^{Q} A'_{Y,k} Y(t - k\tau) + \sum_{k=1}^{R} B'_{Y,k} X(t - k\tau) + \Psi'(t), \end{aligned} \tag{4}$$

where the time step $\tau = \Delta t/L$, i.e., τ is the integer number L times smaller than Δt, $\Xi'(t)$ and $\Psi'(t)$ are independent Gauss noises with the respective variances $\sigma^2_{\Xi'}$ and $\sigma^2_{\Psi'}$. Both UC directions $X \to Y$ and $Y \to X$ should be checked sequentially. For the sake of definiteness, we will test the UC hypothesis $X \to Y$; i.e., we will test the model (1) with $S = 0$. Interestingly, the class M is characterized by four parameters: P, Q, R, and L. The properties of the Gauss processes X and Y are totally determined by their auto- and cross-covariance functions (ACF and CCF) [32]. Resting upon this, we can find the distribution law of sampling estimates of the ACF and CCF for model (4) and, thereby, an analytical criterion of statistical consistency between the CF of the model and the sampling CF of data analyzed.

For the $(P + Q + R + 2)$-dimensional vector of parameters of model (4), we can introduce the notation $\theta' = \left(\left\{A'_{X,k}\right\}_{k=1}^{P}, \left\{A'_{Y,k}\right\}_{k=1}^{Q}, \left\{B'_{Y,k}\right\}_{k=1}^{Q}, \sigma^2_{\Xi'}, \sigma^2_{\Psi'}\right)$. For a specified value of θ', ACF and CCF in model (3) can be determined exactly by solving linear algebraic equations. For the D-dimensional vector of the ACF and CCF in model ($D = 4K + 3$), where $\rho'_{XY}(l\Delta t) = M[X(t)Y(t + l\Delta t)]$, we can introduce the notation $\rho' = \left(\left\{\rho'_{XX}(l\Delta t)\right\}_{l=0}^{K}, \left\{\rho'_{YY}(l\Delta t)\right\}_{l=0}^{K}, \left\{\rho'_{XY}(l\Delta t)\right\}_{l=-K}^{K}\right)$, as well as the notation $\hat{\rho}$ for the vector of sampling estimates of CF obtained for the analyzed time series $\{x_n, y_n\}_{n=1}^N$, i.e., $\hat{\rho}_{XX}(l\Delta t) = (1/N)\sum_{n=1}^{N} y_n y_{n+l}$, $\hat{\rho}_{XY}(l\Delta t) = (1/N)\times \sum_{n=1}^{N} x_n y_{n+l}$. If the analyzed process belongs to the class M

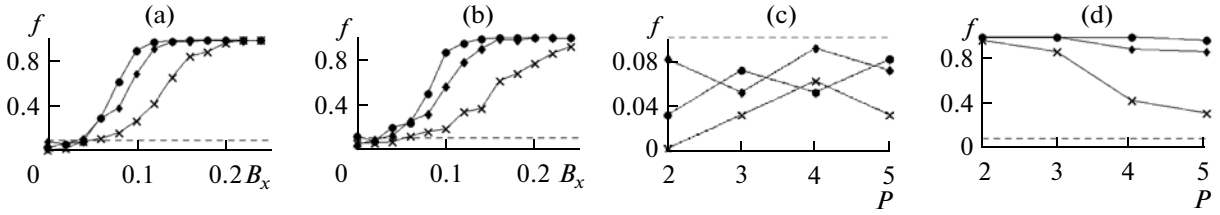

Fig. 4. Frequency of rejection of UC hypothesis for system (2) at $\Delta t = 2$: $N = 1000$ (crosses), $N = 2000$ (diamonds), and $N = 3000$ (circles); (a) $P = 2$, $Q = 2$, $R = 1$; (b) $P = 3$, $Q = 3$, $R = 3$; (c) $B_X = 0$; (d) $B_X = 0.2$ ((c, d) $P = Q$, $R = 1$). At $B_X = 0$, f characterizes the misidentification frequency. The dashed line shows the admissible misidentification frequency at $q = 0.05$ and with accounting for the Bernoulli law for the frequency distribution with ensemble of 100 time series. At $B_X > 0$, f characterizes the sensitivity of the method.

(it corresponds to a certain a priori unknown value $\theta' = \theta'_0$) and N is large, for $\hat{\rho}$ the distribution is characterized by D-dimensional Gauss law with mean ρ' (also corresponding to $\theta' = \theta'_0$) and covariance matrix $\mathbf{C}$, expressed via ρ' according to Barlett's formula [32]. The quantity $\chi^2 = (\hat{\rho} - \rho')^T \mathbf{C} (\hat{\rho} - \rho')$, where T means transposing, is then distributed according to "chi-square" law with D degrees of freedom [32]. Since θ'_0 is a priori unknown, for the purpose of searching for the best model of analyzed processes in the class M, we will determine the minimum value $\hat{\chi}^2_{\min}$ of χ^2 as a function of parameters in the θ' model. If the analyzed process belongs to class M, the quantity $\hat{\chi}^2_{\min}$ is distributed according to chi-square law, but now with $D - D'$ degrees of freedom, since we performed optimization with respect to D' variables. The $(1 - q)$-quantile of this distribution will be denoted through χ^2_{1-q}. If $\hat{\chi}^2_{\min} > \chi^2_{1-q}$, the UC hypothesis is rejected at the significance level q (with the error probability q). Further analysis uses the usual value $q = 0.05$. The K value was assumed to be 20 so that vector $\hat{\rho}$ includes all nonzero values of the ACF and CCF in the examples considered.

The hypothesis can be rejected erroneously if in class M the values P, Q, and R are insufficiently large or the value L is improper. These parameters should be varied in a certain range and the test should be performed again for different P, Q, R, and L. If data are obtained by averaging as is given by (3), this is taken into account in the calculation of ρ' in the model and no other changes in the testing procedure are required.

The efficiency of the test was checked using, e.g., oscillators (2) for $B_Y = 0.3$ and different B_X. For each set of parameters, we generated ensembles of 100 time series with fixed length $N = 1000$, 2000, and 3000 with an ordinary downsampling at $\Delta t = 2$. The value $B_X = 0$ corresponds to UC $X \to Y$ and positive IP $G_{y \to x}$ (see Fig. 2a for $T_Y = 5$). The estimates of $G_{y \to x}$ statistically significantly differ from zero (at 0.05 level according to F-test) with 0.22 probability at $N = 1000$, 0.53 probability at $N = 2000$, and 0.68 probability at $N = 3000$. Thus, misidentifying BC only from IP estimates is very likely. The hypothesis of UC $X \to Y$ was tested for each time series separately for $L = 2$ and for different P, Q, and R in the range from 1 to 5. We calculated the relative frequency f of rejections of zero hypothesis (the fraction of time series in ensemble, for which the hypothesis turned out to be rejected). For $B_X = 0$, this quantity characterizes the misidentifying frequency and, hence, should be no greater than the declared significance level $q = 0.05$ in order for test to be correct. Figures 4a–4d show that this is true even if P, Q, and R are markedly greater than the order of the initial system (2).

At $B_X > 0$, f quantifies the frequency of correct rejections of the UC hypothesis (the sensitivity of the method to BC). The greater f is, the higher the efficiency of the test is. The efficiency grows with increasing B_X and reaches large values if P, Q, and R are not too large (Figs. 4a, 4b). The value of f decreases with diminishing N and growing P, Q, and R (Fig. 4d). This is as expected, because a broader class of models gives a larger probability to find a model with CF close to the observed sampling CF with accuracy to within their estimation errors, which grow with decreasing N. All results are analogous for $\Delta t = 3$ and $\Delta t = 4$ (not shown). Thus, the test works correctly and has sufficiently high sensitivity.

This approach can also be used to describe processes with the help of stochastic differential equations instead of finite-difference equations (4). It is noteworthy that the only difference will be the method for calculating the model values of ρ', which are determined by solving the corresponding system of ordinary differential (and not algebraic) equations. The applicability range of the approach can also be extended to the case of nonlinear systems [35].

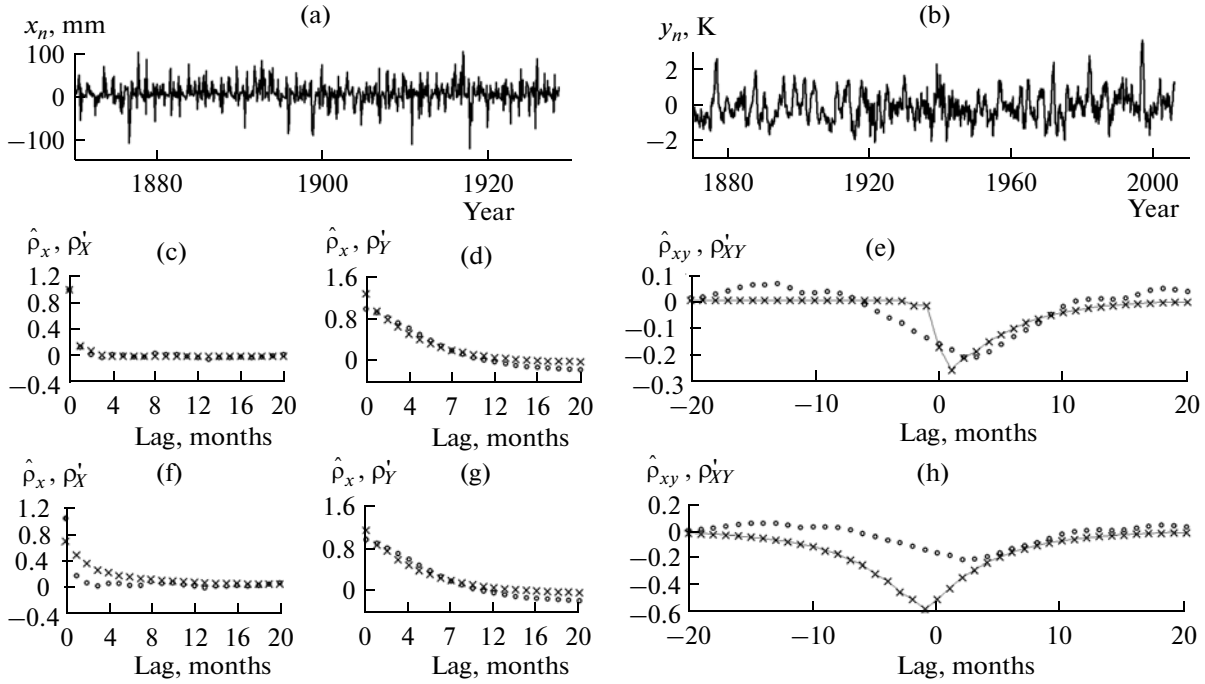

Fig. 5. Analysis of coupling between (a) the Indian Monsoon and (b) the ENSO: (a, b) time series; (c–h) covariance functions of observed data (circles) and model predictions (crosses) with (c–e) UC in the direction "Monsoon → ENSO at $P = Q = 3$, $R = 1$, and $L = 2$ and (f–h) in the direction "ENSO → Monsoon" at $P = Q = 4$, $S = 1$, and $L = 3$.

6. ESTIMATE OF COUPLING BETWEEN THE ENSO AND THE INDIAN MONSOON

This test was also used to verify the earlier conclusion about BC [25, 26] between the ENSO and the Indian Monsoon, i.e., the phenomena with which the processes important in the Asian Pacific region and on a global scale are associated [12, 25, 26, 39, 40]. There are actual reasons for this conclusion on BC, implying that the mechanism acts in both directions. Owing to the formation of anomalies in the sea surface temperature at equatorial Pacific latitudes during El Niño and La Niña events, with the corresponding changes in convective processes, zonal Walker and meridional Hadley circulations, and shift in the Intertropical Convergence Zone, significant seasonal anomalies of temperature and precipitation occur in many regions and, in particular, in the region of the Indian Monsoon. In turn, regimes of the Asian and Australian Monsoons drive circulation features, positions of the regions of intense convection and clouds in zones where El Niño and La Niña form (see, e.g., [25, 26]).

Figure 5 presents the time series of monthly values of x_n for the monsoon index (Fig. 5a), i.e., deseasonalized anomalies in the precipitation amount over India (see, e.g., http://climexp.knmi.nl/data/pALLIN.dat), and y_n for the ENSO index (Fig. 5b), i.e., anomalies in sea surface temperature in the region Niño-3 (see, e.g., http://climexp.knmi.nl/data/iersst_nino3a.dat) for the period of 1871–2006 with the length of time series $N = 1632$ at $\Delta t = 1$ month. An analysis of these time series in [25, 26] with the use of linear AR models gave positive IP in both directions with $G_{y\to x} = 0.020$ and $G_{x\to y} = 0.017$, significantly differing from zero at less than 0.001 level according to F-test. Retaining nonlinear terms did not alter the result by very much. At the same time, it should be noted that these IP values may also be obtained for systems with UC, like in the case with the model system (2), especially when two processes have different relaxation times. The ACF for the monsoon index decreases faster than the ACF for the ENSO index (Figs. 5a, 5b), further motivating a more detailed verification of the type of interrelation between two processes.

The test with the inclusion of averaging (3) was used because we analyzed the monthly total precipitation amount over India and the monthly average sea surface temperature in the region where the ENSO was apparent. We applied only linear AR models (4) because nonlinearity plays a minor role.

We tested the hypothesis about UC for each direction at $L = 2$ (with 2-week "internal" time step τ in the dynamic of the processes), at $L = 3$ (with 10-day step τ), and at $L = 4$ (with 1-week step τ). Timescales of the order of week are characteristic of atmospheric processes. The P, Q, R, and S values were varied in the range from 1 to 5. Both hypotheses about UC turned out to be rejected at the significance level $q < 0.05$ for all models. The best correspondence between model-derived and observed CFs was achieved at $L = 2$, $P = Q = 3$, $R = 1$,

i.e., for "Monsoon → ENSO" UC (Figs. 5c–5e). Unlike the CCF (Fig. 5e), the ACFs of this model (crosses) are quite close to ACFs of the data analyzed. The CCF of data analyzed has the maximum for the time lag of 2 months ("monsoon is master"), but its values for small negative lags are also quite large. Evidently, any model (4) with UC $X \to Y$ may have such a CCF, slowly changing around zero, only if the ACF of process X is simultaneously not as rapidly decreasing as the one in Fig. 5c (circles). Thus, this model may reproduce either the ACF of the monsoon index or the CCF, but not both functions together, indicating the inadequacy of the model with UC "Monsoon → ENSO." The test quantifies the measure of this inadequacy: for the indicated best model (see Figs. 5c–5e), $\hat{\chi}^2_{\min} = 144 >> \chi^2_{0.95} = 95.1$. Models with oppositely directed UC diverge even more strongly from the data analyzed: $\hat{\chi}^2_{\min} = 705 > \chi^2_{0.95} = 92.8$ for the best model with $L = 3$, $P = Q = 4$, $S = 1$ (see Figs. 5f–5h). Thus, the conclusion about BC for the ENSO and the Indian Monsoon has passed an additional test: it is not the result of the sparse sample, at least if the time step of the processes τ is within the range from a week to a month.

7. CONCLUSIONS

We showed how a sparse sample influences the analysis of couplings between climatic processes in terms of time series. In particular, when the sampling interval is quite long, the analysis of the Granger causality may misidentify unidirectional system coupling as BC. Owing to the sparse sample, this effect of "false couplings" shows up in an analysis of variations in the solar radiative flux and global surface temperature. An analysis of data downsampled and averaged over an interval of 3 or 6 months reveals a significant nonzero "influence" of GST on solar activity that is indiscernible from monthly data. We presented a special test for the reliable identification of BC; this test was used to analyze the interaction between the ENSO and the Indian Monsoon. The previous conclusion about the mutual influence of these processes is confirmed by this test, at least at the time steps from a week to a month under analysis here.

The test, which is suggested to confirm or reject the speculations on the type of coupling between processes, can be implemented in describing the processes with the help of differential equations resting upon physical model-based considerations with quite a wide applicability range. This test seems to be potentially useful for judiciously studying the interaction of climatic processes with the verification of conclusions on BCs, as was done in this work. A relevant broader scope treatment of causality in the presence of three or more interacting processes requires special studies.

ACKNOWLEDGMENTS

This work was supported by the Russian Foundation for Basic Research (grant nos. 11-02-00599, 11-05-01139, 12-05-91057-NTsNI, and 12-05-91323-SIG), programs of the Russian Academy of Sciences and the Ministry of Education and Science of the Russian Federation (state contracts 11.519.11.5004), and by grant from the President of the Russian Federation NSh-5467.2012.5.

REFERENCES

1. H. F. Blanford, "On the connection of the Himalaya snowfall with dry winds and seasons of drought in India," Proc. R. Soc. (London), **37**, 1–23 (1884).
2. G. T. Walker and E. W. Bliss, "World weather V," Mem. R. Meteorol. Soc. **4** (36), 53–84 (1932).
3. R. H. Kripalani and A. Kulkarni, "Rainfall variability over Southeast Asia: Connections with Indian Monsoon and ENSO extremes: new perspectives," Int. J. Climatol. **17** (11), 1155–1168 (1997).
4. J. Huang, K. Higuchi, and A. Shabbar, "The relationship between the North Atlantic Oscillation and the ENSO," Geophys. Res. Lett. **25**, 2707–2710 (1998).
5. K. Arpe, L. Bengtsson, G. S. Golitsyn, I. I. Mokhov, V. A. Semenov, P. V. Sporyshev, "Analysis and modeling of the hydrological regime variations in the Caspian Sea basin," Dokl., Earth Sci. **366** (4), 552–556 (1999).
6. G. V. Gruza, E. Ya. Ran'kova, L. K. Kleshchenko, and E. N. Aristova, "Relation of climatic anomaly in Russia with ENSO," Meteorol. Gidrol., No. 5, 32–51 (1999).
7. I. I. Mokhov, V. A. Bezverkhny, and A. A. Karpenko, "Evolution of climatic characteristics and atmospheric components at Milankovitch scales from Vostok ice core," in *Research Activities in Atmospheric and Oceanic Modelling*, Ed. by H. Ritchie, WMO/TD-No.1105, pp. 2.17–2.18 (2002).
8. S. Jevrejeva, J. C. Moore, and A. Grinsted, "Influence of the Arctic Oscillation and El Niño–Southern Oscillation (ENSO) on ice conditions in the Baltic Sea: The wavelet approach," J. Geophys. Res. **108** (D21), 4677 (2003). doi 10.1029/2003jd003417
9. A. Grinsted, J. C. Moore, and S. Jevrejeva, "Application of the cross wavelet transform and wavelet coherence to geophysical time series," Nonlin. Processes Geophys. **11**, 561–566 (2004).
10. W. Wang, B. T. Anderson, R. K. Kaufmann, and R. B. Myneni, "The relation between the North Atlantic Oscillation and SSTs in the North Atlantic basin," J. Clim. **17** (24), 4752–4759 (2004).
11. I. I. Mokhov, V. A. Bezverkhnii, and A. A. Karpenko, "Diagnosis of relative variations in atmospheric greenhouse gas contents and temperature from Vostok Antarctic ice-core paleoreconstructions," Izv., Atmos. Ocean. Phys. **41** (5), 523–536 (2005).
12. D. Maraun and J. Kurths, "Epochs of phase coherence between El-Nino/Southern Oscillation and Indian Monsoon," Geophys. Res. Lett. **32**, L15709 (2005). doi 10.1029/2005GL023225
13. I. I. Mokhov and D. A. Smirnov, "Study of the mutual influence of the El Niño–Southern Oscillation pro-

cesses and the North Atlantic and Arctic oscillations," Izv., Atmos. Ocean. Phys. **42** (5), 598–614 (2006).

14. I. I. Mokhov and D. A. Smirnov, "El-Niño Southern Oscillation drives North Atlantic Oscillation as revealed with nonlinear techniques from climatic indices," Geophys. Res. Lett. **33**, L03708 (2006). doi 10.1029/2005GL024557
15. T. J. Mosedale, D. B. Stephenson, M. Collins, et al., "Granger causality of coupled climate processes: Ocean feedback on the North Atlantic Oscillation," J. Clim. **19** (7), 1182–1194 (2006).
16. M. Palus and D. Novotna, "Quasi-Biennial Oscillations extracted from the monthly NAO index and temperature records are phase-synchronized," Nonlin. Processes Geophys. **13**, 287–296 (2006).
17. P. F. Verdes, "Global warming is driven by anthropogenic emissions: A time series analysis approach," Phys. Rev. Lett. **99** (4), 048501 (2007).
18. I. I. Mokhov and D. A. Smirnov, "Diagnostics of a cause–effect relation between solar activity and the Earth's global surface temperature," Izv., Atmos. Ocean. Phys. **44** (3), 263–272 (2008).
19. S. S. Kozlenko, I. I. Mokhov, and D. A. Smirnov, "Analysis of the cause and effect relationships between El Niño in the Pacific and its analog in the equatorial Atlantic," Izv., Atmos. Ocean. Phys. **42** (6), 704–713 (2009).
20. S. Bronnimann, "Impact of El-Niño-Southern Oscillation on European climate," Rev. Geosci. **45**, RG3003 (2007). doi 10.1029/2006RG0001999
21. I. I. Mokhov and D. A. Smirnov, "Empirical estimates of the influence of natural and anthropogenic factors on the global surface temperature," Dokl. Earth Sci. **427** (5), 798–803 (2009).
22. R. Lu, W. Chen, and B. Dong, "How does a weakened Atlantic thermohaline circulation lead to an intensification of the ENSO–South Asian Summer Monsoon interaction?," Geophys. Res. Lett. **35**, L08706 (2008). doi 10.1029/2008GL033394
23. D. A. Smirnov and I. I. Mokhov, "From Granger causality to long-term causality: Application to climatic data," Phys. Rev. E **80**, 016208 (2009). doi 10.1103/PhysRevE.80.016208
24. V. I. Byshev, V. G. Neiman, and Yu. A. Ivanov, "Natural factors of global variability in modern climate," *Izv. Akad. Nauk, Ser. Geogr.,* No. 1, 7–13 (2009).
25. I. I. Mokhov, D. A. Smirnov, P. I. Nakonechny, et al., "Alternating mutual influence of El-Niño/Southern Oscillation and Indian Monsoon," Geophys. Res. Lett. **38**, F04 (2011). doi 10.1029/2010GL045932
26. I. I. Mokhov, D. A. Smirnov, P. I. Nakonechnyi, et al., "Relationship between El-Niño/Southern Oscillation and the Indian Monsoon," Izv., Atmos. Ocean. Phys. **48** (1), 47–56 (2012).
27. W. Chen, B. Dong, and R. Lu, "Impact of the Atlantic Ocean on the multidecadal fluctuation of El Niño–Southern Oscillation-South Asian Monsoon relationship in a coupled general circulation model," J. Geophys. Res. **115**, D17109 (2010). doi 10.1029/2009JD013596
28. I. I. Mokhov, D. A. Smirnov, and A. A. Karpenko, "Assessments of the relationship of changes of the global surface air temperature with different natural and anthropogenic factors based on observations," Dokl. Earth Sci. **443** (1), 381–387 (2012).
29. C. W. J. Granger, "Investigating causal relations by econometric models and cross-spectral methods," Econometrica **37** (3), 424–438 (1969).
30. C. A. Sims, "Discrete approximations to continuous time distributed lags in econometrics," Econometrica **39**, 545–563 (1971).
31. M. Marcellino, "Some consequences of temporal aggregation in empirical analysis," J. Bus. Econ. Stat. **17**, 129–136 (1999).
32. G. Box and G. Jenkins, *Time Series Analysis: Forecasting and Control* (Freeman, San Francisco, 1970).
33. G. Schwarz, "Estimating the dimension of a model," Ann. Stat. **6** (2), 461–464 (1978).
34. G. Seber, *Linear Regression Analysis* (Wiley, New York, 1977).
35. D. A. Smirnov and B. P. Bezruchko, "Spurious causalities due to low temporal resolution: Towards detection of bidirectional coupling from time series," Europhys. Lett. **100** (1), 10005 (2012). doi 10.1209/0295-5075/100/100005
36. J. Timmer, M. Lauk, W. Pfleger, and G. Deuschl, "Cross-spectral analysis of physiological tremor and muscle activity: I. Theory and application to unsynchronized electromyogram," Biol. Cybern. **78**, 349–357 (1998).
37. J. Lean, G. Rottman, J. Harder, and G. Kopp, "Source contributions to new understanding of global change and solar variability," Solar Physics. **230** (1–2), 27–53 (2005).
38. D. V. Hoyt and K. H. Schatten, *The Role of the Sun in Climate Change* (Oxford Univ. Press, Oxford, 1997).
39. *Climate Change 2007: The Physical Science Basis*, Ed. by S. Solomon, D. Qin, M. Manning, Z. Chen, M. Marquis, K. Averyt, M. Tignor and H. Miller (Cambridge University Press, Cambridge, New York, 2007).
40. K. Yamasaki, A. Gozolchiani, and S. Havlin, "Climate networks around the globe are significantly affected by El-Niño," Phys. Rev. Lett. **100**, 228501 (2008).

Translated by O. Bazhenov